Band Structure and Transport Properties of CrO_2

Steven P. Lewis
Department of Chemistry, University of Pennsylvania, Philadelphia, Pennsylvania 19104

Philip B. Allen
Department of Physics, State University of New York, Stony Brook, New York 11794-3800

Taizo Sasaki
National Researach Institute for Metals, 1-2-1 Sengen, Tsukuba 305, Japan
(February 8, 2008)

Local Spin Density Approximation (LSDA) is used to calculate the energy bands of both the ferromagnetic and paramagnetic phases of metallic CrO_2. The Fermi level lies in a peak in the paramagnetic density of states, and the ferromagnetic phase is more stable. As first predicted by Schwarz, the magnetic moment is 2 μ_B per Cr atom, with the Fermi level for minority spins lying in an insulating gap between oxygen p and chromium d states ("half-metallic" behavior.) The A_{1g} Raman frequency is predicted to be 587 cm^{-1}. Drude plasma frequencies are of order 2eV, as seen experimentally by Chase. The measured resistivity is used to find the electron mean-free path ℓ which is only a few angstroms at 600K, but nevertheless, resistivity continues to rise as temperature increases. This puts CrO_2 into the category of "bad metals" in common with the high T_c superconductors, the high T metallic phase of VO_2, and the ferromagnet $SrRuO_3$. In common with both $SrRuO_3$ and Sr_2RuO_4, the measured specific heat γ is higher than band theory by a renormalization factor close to 4.

I. INTRODUCTION

The physical properties of rutile-structure oxides are diverse, including insulators (TiO_2), antiferromagnets (MnO_2), good metals (RuO_2), and metal-insulator systems (VO_2). Metallic CrO_2, with a Curie temperature $T_C \approx 390$K, is the only ferromagnet in this class. Schwarz [1] used LSDA band theory to predict that the spin moment would be the full 2 μ_B required by Hund's rules for the Cr^{4+} ($3d^2$) ion. The Fermi level lies in a partly filled (metallic) band for the majority (up spin) electrons, but for minority (down) spins lies in a semiconducting gap which separates the filled oxygen p levels from the Cr d levels. The situation where one spin species is metallic and the other semiconducting has been named "half-metallic" by de Groot *et al.* [2]. Evidence of close to 100% spin polarization was seen in both spin-polarized photoemission [3] and vacuum tunneling [4]. However, this polarization was observed not at the Fermi energy, but 2eV below. Brändle *et al.* [5] found good agreement between theory and experiment for the diagonal parts of the optical conductivity tensor, but less good for the off-diagonal magnetoconductivity properties. These discrepancies have not yet been resolved.

Besides the paper of Schwarz [1], LSDA band structure calculations have been reported by several other groups [6–8], with similar results. We repeat these LSDA calculations using a plane-wave pseudopotential (PWPP) method, and give both a prediction of the frequency of the $Q = 0$ Raman active optic mode of A_{1g} symmetry and an analysis of transport measurements using band-theoretical parameters. This work is one of the first illustrations of the ability of a plane-wave pseudopotential technique to do a highly accurate LSDA calculation, and the first, to our knowledge, for a ferromagnetic compound.

II. COMPUTATIONAL METHOD

The electronic ground state for CrO_2 is computed using the local spin density approximation [9] (LSDA) of density functional theory [10]. The form chosen for the exchange-correlation energy and potential is that of Ceperley and Alder [11]. We make the frozen-core approximation in which the core electrons are fixed in their free-atom configuration, and only the valence electrons are allowed to respond to the chemical environment of the solid. Interactions between

the valence electrons and ion cores are described by efficient [12] norm-conserving pseudopotentials [13]. The single-particle wavefunctions are expanded in a plane-wave basis set which is well-converged for CrO_2 at a cutoff energy of 81 Ry.

A worry with the PWPP method is that, because spin-splitting of the exchange-correlation potential is driven largely by the tightly-bound d-electrons, spin-polarizing effects would be prominent in the core region where the pseudo wavefunctions differ significantly from the all-electron wavefunctions. However, Sasaki, *et al.*, have recently demonstrated [14] that this is not, in fact, a problem. While the pseudopotential approach does cause the $3d$ wavefunction to shift in the core region relative to the all-electron case, it also produces a similar shift in the spin-splitting of the exchange-correlation potential. Thus the total energy, which involves integration of the density against the potential, is largely unaffected. Sasaki, *et al.*, have also shown that it is important to employ the partial-core correction scheme of Louie, *et al.* [15] in order to reduce core-valence overlap errors introduced by nonlinearity of the exchange-correlation potential. Spin-polarized calculations using this method have been performed for atomic and bulk iron and nickel, and the agreement with all-electron LSDA calculations for structural, electronic, and magnetic properties is outstanding [14].

To our knowledge, the present study of CrO_2 is the first LSDA investigation of a magnetic compound using the PWPP method. Results for the magnetic and electronic structure obtained here are in excellent agreement with previous all-electron LSDA band-structure calculations of this system [1,6–8], which nicely illustrates the effectiveness and accuracy of this method.

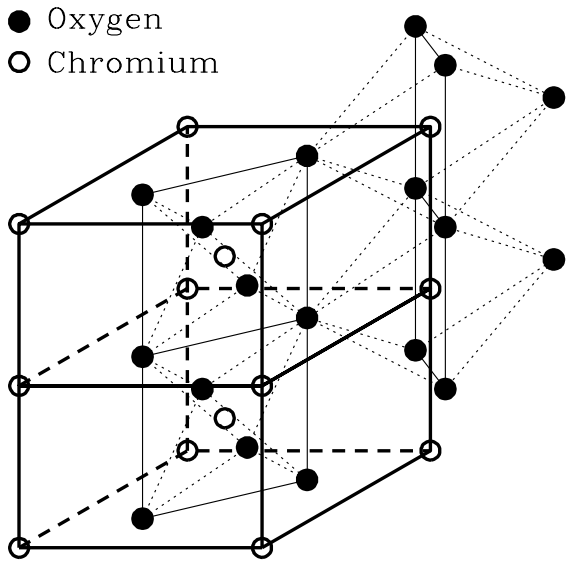

FIG. 1. Illustration of the rutile structure. Heavy solid and dashed lines demarcate unit cells of the crystal. Thin lines emphasize the oxygen octahedra surrounding each chromium atom, with solid lines highlighting the equatorial planes and dotted lines linking them to the apical oxygen atoms.

The rutile structure (see Fig. 1) has a simple tetragonal Bravais lattice with two formula units per unit cell. It consists of chromium atoms octahedrally coordinated by oxygen atoms, with the oxygen octahedra arranged in "ribbons" running parallel to the tetragonal c-axis. Adjacent octahedra on the same ribbon share a common edge, whereas octahedra on adjacent ribbons share a common corner and are situated relative to each other according to a four-fold screw axis with non-primitive translation equal to half the c-axis. Figure 1 highlights the planar CrO_4 units which form the ribbons. We refer to the ribbon oxygens as "equatorial" and the other two oxygens of the CrO_6 octahedra as "apical." The octahedra are orthorhombically distorted away from the ideal geometry, with the apical oxygen atoms slightly more distant from the central chromium atom than the equatorial oxygen atoms. Chromium atoms are located at the positions $[0,0,0]$ and $[\frac{1}{2},\frac{1}{2},\frac{1}{2}]$ in lattice coordinates, and the four oxygen atoms are located at $[u,u,0]$, $[1-u,1-u,0]$, $[\frac{1}{2}+u,\frac{1}{2}-u,\frac{1}{2}]$, and $[\frac{1}{2}-u,\frac{1}{2}+u,\frac{1}{2}]$, where u is a dimensionless internal coordinate. The measured values of the structural parameters, a, c, and u, are 4.419Å, 2.912Å, and 0.303, respectively [16]. In the

present study, we have fixed the axes at their experimental lengths and have opitimized the internal coordinate, u. Its computed value is 0.3043, in excellent agreement with experiment. The irreducible wedge of the tetragonal Brillouin zone has been sampled at 9 k-points for the purposes of computing the self-consistent electron density. The electronic density of states, magnetic moment, Fermi energy, Fermi surface area, and transport coefficients are determined using the linear tetrahedron method [17] on band energies computed at 50 irreducible k-points.

III. ELECTRONIC STRUCTURE

Figure 2 shows the computed electronic density of states (DOS) of ferromagnetic CrO_2 for majority spins (positive axis) and minority spins (negative axis). These results agree well with earlier DOS calculations for this material [1,6–8]. Integrating the total DOS up to the total number of valence electrons determines the Fermi energy, which is then used as the zero of energy. The Fermi level intersects the majority spin bands near a local minimum in the DOS and lies in a band gap of the minority-spin DOS. Thus CrO_2 is half-metallic within LSDA, as was first demonstrated by Schwarz [1]. This property leads to an integral magnetic moment, which is found to be 2 μ_B/CrO_2, the value predicted by Hund's rules for the spin moment of the Cr^{4+} ion. The density of majority states at the Fermi level is 0.69 states/eV/CrO_2.

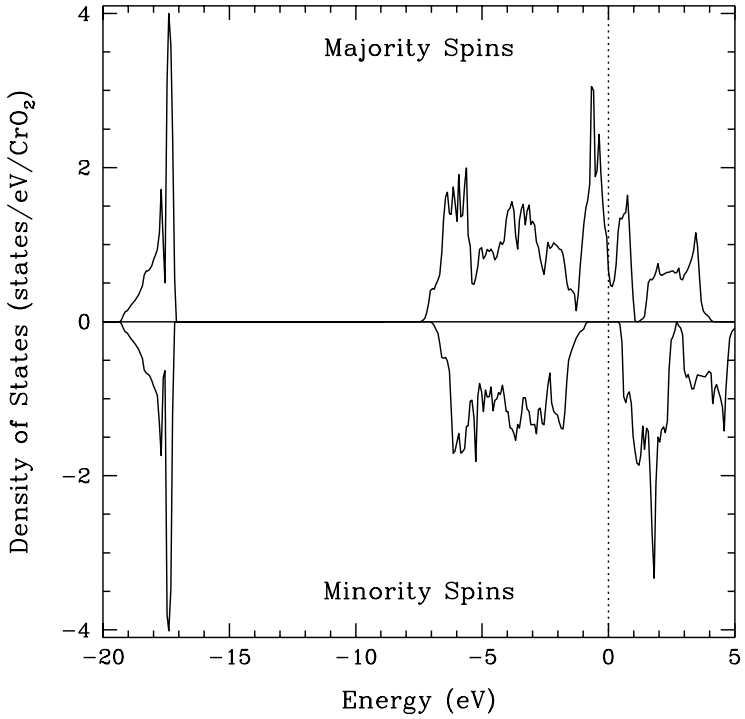

FIG. 2. Densities of states for majority and minority spins in ferromagnetic CrO_2. Majority (minority) states are plotted along the positive (negative) ordinate. The dotted line denotes the Fermi energy.

Contour plots for the spin density ($s(\vec{r}) = n_\uparrow(\vec{r}) - n_\downarrow(\vec{r})$) are shown in Fig. 3 for two cross-sections of the crystal. Fig. 3(a) contains the $(1\bar{1}0)$ plane formed by the equatorial oxygen atoms and the chromium atom. Fig. 3(b) shows a perpendicular plane containing two apical and two equatorial oxygen atoms. Both panels have the same contour-level spacing. These figures reveal that the spin density is highly localized around the chromium atom, and that it stems almost exclusively from the chromium $3d$ states. Fig. 3(a) shows that the spin density has the "cloverleaf" shape of a d_{xy} function, where a local set of x, y, and z axes are used with the origin on a Cr atom and axes toward the octahedral O atoms, the axial oxygen defining the local z-axis. It is well-known that the crystal field caused by an octahedron of surrounding negative charges splits the d states of a transition metal ion, with the three t_{2g} states (d_{xy}, d_{yz}, and d_{zx}) lying lower and the two e_g states ($d_{x^2-y^2}$ and $d_{3z^2-r^2}$) lying higher. Fig. 3(b) shows that the d_{xz}, or equivalently, the d_{yz} component of $s(\vec{r})$ is also present with about half the strength of the d_{xy} component. The e_g states make no noticeable contribution.

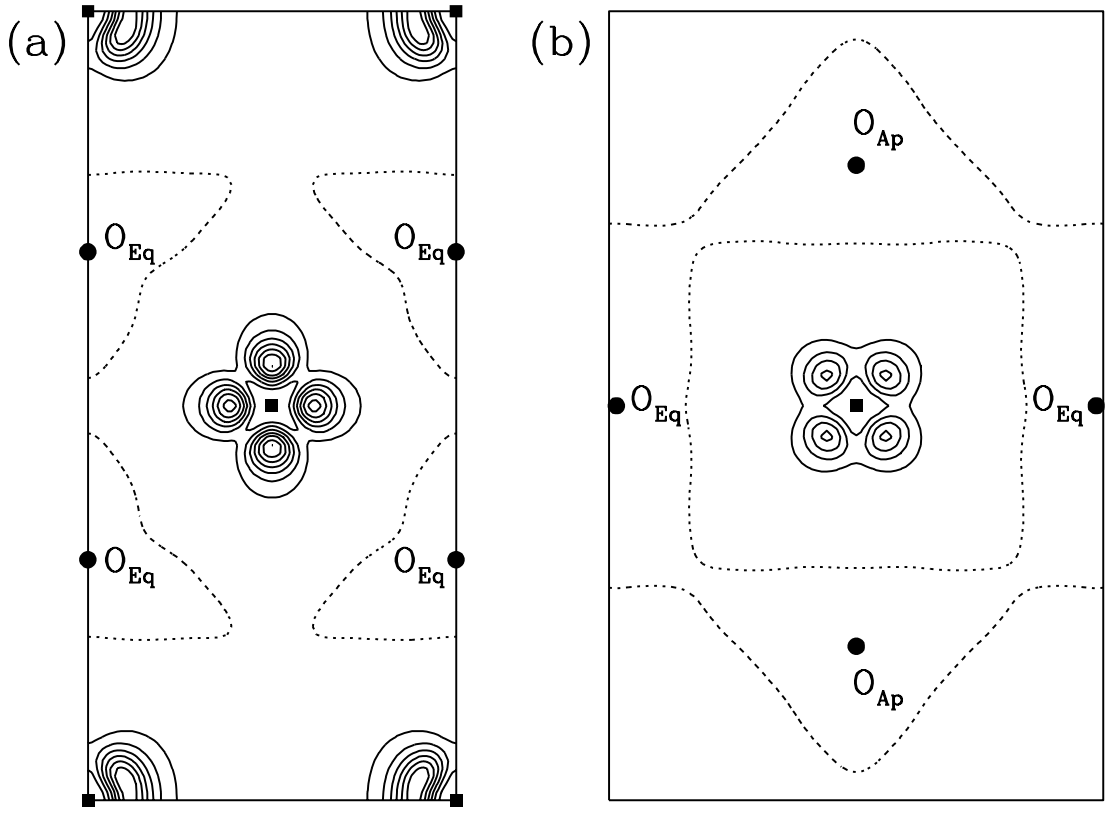

FIG. 3. Spin density of CrO_2 in (a) the equatorial plane of the oxygen octahedron and (b) a plane of the octahedron containing two apical and two equatorial oxygens. Adjacent contour levels are separated by 30 μ_B/unit cell, with the zero contour designated by dashed lines. Chromium and oxygen atomic positions are designated by filled squares and circles, respectively. Apical and equatorial oxygen atoms are distinguished by labels.

Bonding in CrO_2 has been analyzed by Sorantin and Schwarz [21] and by Burdette *et al.* [22]. Referring to the DOS in Fig. 2, the sharp band at about -17 eV arises from the oxygen 2*s* level, and is identical for both spin species, contributing nothing to the spin density. Similarly, the broad band from -7 to -1 eV comes mostly from the oxygen 2*p* states, with a small admixture of chromium 3*d* character, and is almost identical for majority and minority spins. The source of the spin density is an exchange splitting of approximately 1.8 eV of the broad bands near and above the Fermi level. These bands are primarily chromium 3*d* states of t_{2g} parentage, with the e_g bands higher in energy by the crystal-field splitting of approximately 2.5 eV. The exchange splitting shifts the minority spin *d*-bands above the Fermi level. The majority t_{2g} band is two-thirds filled, with the Fermi level lying in a "pseudogap" in the t_{2g} manifold. Following Sorantin and Schwarz, we can explain the stability and the shape of the spin density in CrO_2 as follows. Only one of the three t_{2g} states participates in covalent oxygen *p*- chromium *d* hybridization. Hybridization creates both a bonding and an antibonding hybrid orbital, with the bonding orbital reduced in energy, appearing in the occupied region of nominally oxygen *p* states, and the antibonding hybrid orbital remaining in the chromium t_{2g} manifold, but pushed up in energy relative to the two non-bonding members, leaving the "pseudogap". To see which t_{2g} state hybridizes, consider an oxygen atom with its three coplanar chromium nearest neighbors. This Cr_3O cluster builds σ-bonds from hybrids between the two Cr e_g states and two of the three O *p* states. (This hybridization leaves antibonding e_g states raised in energy relative to t_{2g} states, and is part of the explanation of the crystal-field splitting.) The leftover O *p* state is the one which points perpendicular to the Cr_3O plane. This state hybridizes by forming a π-bond with the Cr t_{2g} state which is correctly oriented. This state is orthogonal to the d_{xy} state which lies in the equatorial plane. Thus one half of the d_{yz} and d_{zx} components of the t_{2g} manifold is pushed upward by antibonding, and this explains the dominance of d_{xy} character in the spin density.

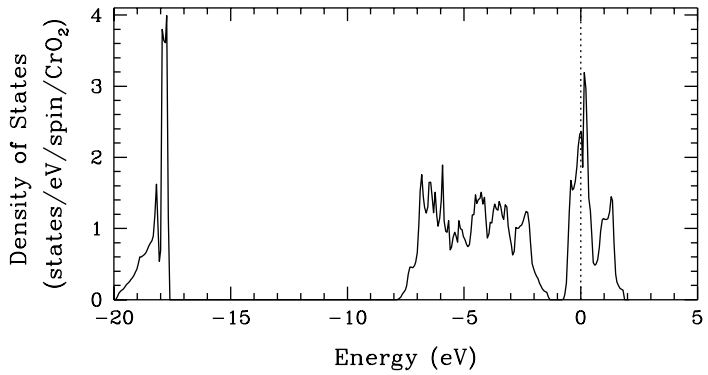

FIG. 4. Density of states for paramagnetic CrO_2. The dotted line denotes the Fermi energy.

For comparison purposes, we have also computed the band structure for CrO_2 without spin polarization. The DOS for paramagnetic CrO_2 is plotted in Fig. 4. It agrees fairly well with the LMTO calculation of Kulatov and Mazin [6], although they did not find a pseudogap in the chromium t_{2g} band. Note that the Fermi level intersects a sharp peak of the DOS. The large DOS at the Fermi level (2.35 states/eV/CrO_2/spin) is an unstable, high-energy situation, which is relieved by the formation of a ferromagnetic phase, according to the usual Stoner argument. The paramagnetic band structure also provides a useful comparison for understanding the electronic transport properties of CrO_2, as is discussed later.

IV. RAMAN MODE

A symmetry analysis of the zone-center phonons of the rutile structure (space group $P4_2/mnm$) shows that there are four Raman frequencies and four infrared-active frequencies. The Raman frequencies belong to irreducible representations A_{1g}, A_{2g}, A_{3g}, and E_g, whereas one of the IR frequencies has A_{4u} symmetry, with the rest having E_u symmetry.

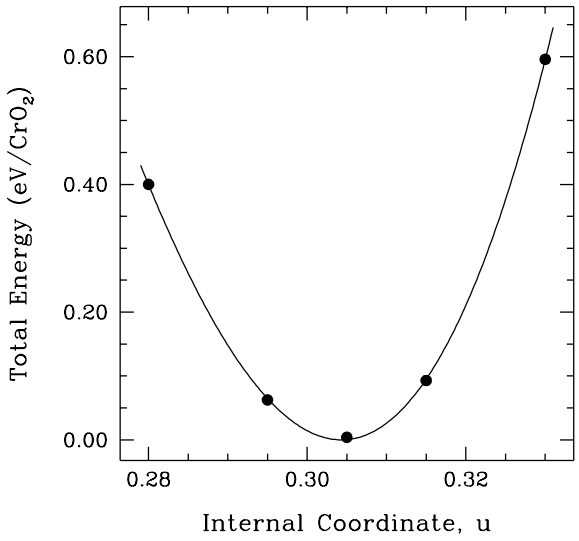

FIG. 5. Total energy *versus* internal coordinate u for fixed values of lattice parameters a and c.

The A_{1g} Raman mode is particularly simple, corresponding to fluctuations of the internal coordinate, u. Thus, the energy of this mode is a by-product of a calculation of the equilibrium structure. Figure 5 shows the variation of the total energy of the crystal as a function of u, for fixed values of the lattice constants, a and c. The solid line passing

through the data points is a cubic-polynomial fit to the data, with the zero of energy placed at the minimum. As mentioned above, the equilibrium value of u is predicted to be 0.3043. From the curvature of this function at the minimum, we predict the frequency of the A_{1g} Raman mode to be 587 cm^{-1}. To our knowledge, this quantity has not yet been measured.

V. SPECIFIC HEAT

The low temperature specific heat $C = \gamma T$ was measured [20] as γ=7 mJ K^{-2} per mole CrO_2. Using independent electron theory, $\gamma = (\pi^2 {k_B}^2/3)N_\gamma(0)$, this corresponds to an effective density of states $N_\gamma(0)$=3.0 states/eV per CrO_2 molecule. This exceeds our calculated $N(0)$=0.69 by a factor $1 + \lambda_\gamma$=4.3, a large enhancement. Conventional metals have an enhancement $1 + \lambda$ from electron-phonon interactions, and it would be possible to have λ from this source fairly large, perhaps as big as 1, but not as big as 3.3. Analogous to the electron-phonon enhancement, ferromagnetic metals can have a mass enhancement from virtual exchange of spin fluctuations. Because of the absence of single particle states of opposite spin from the spectrum at the Fermi energy, this source is expected to be altered in a half-metallic material [23]. Perhaps one could patch up band theory in some way, improving the LSDA exchange-correlation potentials or making self-interaction or gradient corrections, to diminish the enhancement to a more reasonable value. However, given the reasonable success of LSDA in describing the total energy and the qualitative nature of the spectrum of electronic excitations farther away from the Fermi surface, it seems to us more likely that the large specific heat enhancement indicates a correlation effect beyond the reach of a patched-up density-functional theory. Very similar enhancements have been reported in the ferromagnet $SrRuO_3$ [24] and in Sr_2RuO_4 [25]

VI. RESISTIVITY

Transport properties of ferromagnets have been reviewed by Campbell and Fert [26]. The electrical resistivity of single crystal samples of CrO_2 was measured by Redbell *et al.* [19]; the data are transcribed on Fig. (6). Similar results were reported by Chamberland [27]. The solid curves on Fig. (6) are Bloch-Grüneisen fits to the low-temperature data.

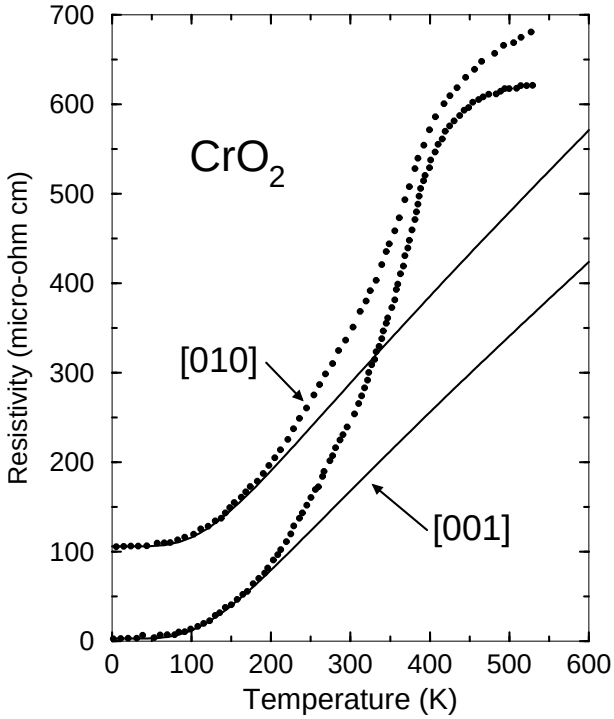

FIG. 6. Resistivity of CrO_2 measured in ref. [19]. The data for the [010] direction have been shifted up by 100 $\mu\Omega$cm for clarity. The solid curves are Bloch-Grüneisen functions fitted to the low T data as explained in the text.

In order to interpret the resistivity curves, it is useful to choose Ni and Nb as reference materials exhibiting canonical resistivity behavior. The data, shown on Fig. (7), are from Refs. [28–31] for Ni and from Ref. [32] for Nb. Boltzmann transport theory evaluates the current by summing up the velocity of the occupied quasiparticle states. Rather than solving the Boltzmann equation for the quasiparticle distribution function, it is usually a reasonable approximation to use the *ansatz* that the distribution function F is a displaced Fermi Dirac distribution, $F_s(\vec{k}) = f(\epsilon_s(\vec{k} + e\vec{E}\tau_s/\hbar))$. The spin state is labeled by $s =\uparrow$ or $\downarrow$. This yields a formula for the conductivity,

$$\sigma_{xx} = e^2 N_\uparrow(0)\langle v_{x\uparrow}^2\rangle\tau_{xx\uparrow} + e^2 N_\downarrow(0)\langle v_{x\downarrow}^2\rangle\tau_{xx\downarrow} \tag{1}$$

where the angular brackets signify a Fermi surface average $\langle g\rangle \equiv \sum_k g(k)\delta(\epsilon_k)/\sum_k \delta(\epsilon_k)$. The temperature dependence of the resistivity is controlled by the scattering times $\tau_{\alpha\beta s}$. For electron-phonon scattering, this can be modelled by the Bloch-Grüneisen formula,

$$\hbar/\tau_{xxs} = 4\pi k_B T \int_0^{\omega_D} \frac{d\Omega}{\Omega}\alpha_{xxs}^2 F(\Omega)\left[\frac{\hbar\Omega/2k_BT}{\sinh(\hbar\Omega/2k_BT)}\right]^2 \tag{2}$$

where the Debye model $\alpha_{xxs}^2 F(\Omega) = 2\lambda_{xxs}(\Omega/\omega_D)^4$ is used. If the quasiparticle properties $N_s(0)$ and $\langle v_{xs}^2\rangle$ are known, then the parameters needed to fit data are λ_{xxs} and $\Theta_D = \hbar\omega_D/k_B$.

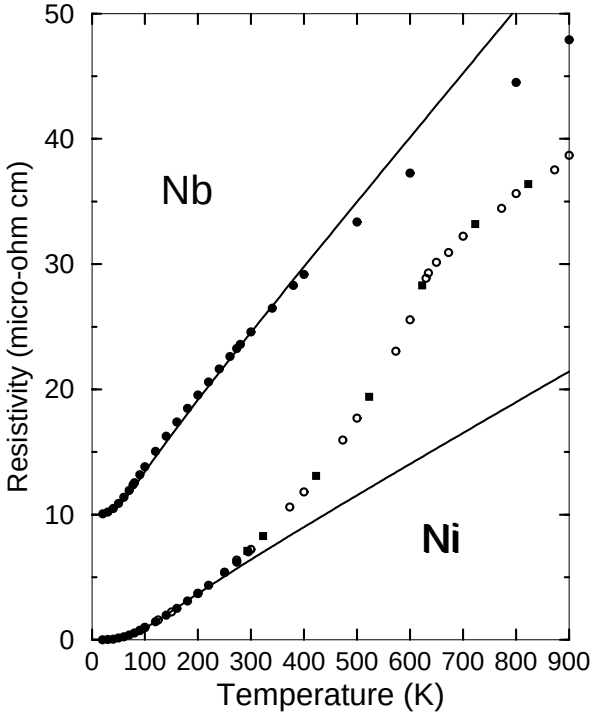

FIG. 7. Resistivity of Ni and Nb *versus* temperature showing canonical behavior of ferromagnetic and nonmagnetic metals. The data for Ni are from Ref. [28] (filled circles), Ref. [29] (open circles), Ref. [30] (filled squares), and Ref. [31] (open squares.) The data for Nb, from Ref. [32], have been shifted up by 10 $\mu\Omega$cm for clarity. The solid curves are Bloch-Grüneisen functions as explained in the text.

The simplest case to model is Nb, a cubic paramagnet, so that all Cartesian directions and both spin directions have the same value of λ_{xxs}, denoted $\lambda_{\rm tr}$. It is convenient to define a "Drude plasma frequency" tensor Ω_P by

$$\Omega_{Pxx}^2 = 4\pi e^2 \sum_s N_s(0)\langle v_{xs}^2\rangle \tag{3}$$

Using $\hbar\Omega_P$=9.12eV for Nb as calculated by Papaconstantopoulos [33], Θ_D = 275K from the low T specific heat [34], and setting $\lambda_{\rm tr}$ equal to the superconducting λ=1.05 found in tunneling [35], the Bloch-Grüneisen curve shown in

Fig. (7) follows with no adjustable parameters. A slightly better fit could be produced by reducing the value of Θ_D, which would accord with knowledge from tunneling about the actual effective phonon frequencies. The fit is good up to 500K, beyond which the data slowly turn downward below the theory, probably signalling the onset of "saturation" [36]. In many elemental d-band metals and intermetallic compounds, when the electron mean-free path ℓ becomes less than 10Å, the thermal increase of resistivity is slowed. When the mean free path would hypothetically (according to Boltzmann theory) become as short as 5Å, the temperature dependence is almost completely arrested. Boltzmann theory is expected to fail when ℓ is not large compared with a lattice spacing. Typically this occurs when the resistivity is within a factor of 2 of $100\mu-\Omega$cm. From the known parameters of Nb, it is predicted that ℓ (defined as $\langle v^2\rangle^{1/2}\tau$) at 500K should be 14.5Å, close to (but a little higher than) where "saturation" is expected.

An objection to the procedure used here is that Boltzmann theory needs the velocities of the band quasiparticles, while the single-particle energies ϵ_k calculated using LSDA band theory are not guaranteed to have any physical meaning. The only reliable test of this objection is comparison of LSDA eigenenergies with experimental quasiparticle properties. Tests for the resistivity of paramagnetic metals have generally worked very well [37], similar to the result seen here in Nb.

Nickel is a cubic ferromagnet (T_C=627K) so there are two electron-phonon parameters, $\lambda_\uparrow$ and $\lambda_\downarrow$. The resistivity cannot be fit with Bloch-Grüneisen curves; above 200K extra scattering occurs because of fluctuating spins. If we assume that below 200K electron-phonon scattering dominates, we can still not determine separately all the constants of a Bloch-Grüneisen curve, because at temperatures much less than Θ_D only a single combination, $\lambda/\Omega_P^2\Theta_D^4$ enters the expression. To get a rough idea, we make the model $\lambda_\uparrow=\lambda_\downarrow$ and take Θ_D=450K from low T specific heat. Using the joint up and down spin Drude plasma frequency Ω_P=6.96eV [33], the Bloch-Grüneisen curve drawn on Fig. (7) corresponds to the choice λ=0.27. This is a reasonable value, intermediate between the values 0.13 and 0.47 found for the related metals Cu and Pd [37], and agrees with the result λ=0.24 found in the pioneering calculation of Yamashita *et al.* [38]. It would also be reasonable to choose a lower value of Θ_D, obtaining a correspondingly reduced value of λ, and a fit which follows the experimental $\rho(T)$ up to a somewhat smaller temperature. From the measured specific heat and the band values of Papaconstantopoulos, one finds $\lambda_\gamma\approx 0.70$, significantly bigger than can be reconciled with resistivity, and suggesting that there is an additional source of renormalization beyond electron-phonon effects.

In principle, Boltzmann theory should still work for Ni at temperatures up to at least T=900K. If only the electron-phonon mechanism were causing scattering, then the value λ=0.27 implies that the mean-free path for up spin electrons would be 35Åand for down spin electrons it would be 12Å, using the Fermi velocities found by Papaconstantopoulos [33]. However, the actual resistivities, because of spin scattering, are higher by 1.72 than the electron-phonon fit, so the corresponding mean-free paths are reduced to 20Åand 7Å. But at 900K Ni is no longer a ferromagnet, and separate up and down spin Fermi surfaces no longer exist. Nevertheless, the mean free paths suggested by this analysis are long enough that it seems likely that the basic premises of Boltzmann theory are not badly violated. The fact that $\rho(T)$ continues to increase with temperature at 900K suggests a metal where transport is still governed by propagating quasiparticles which scatter more rapidly at higher T.

We now apply this kind of analysis to CrO_2. At low T, there are only majority (up) spins at the Fermi surface, and thus only two electron-phonon parameters, λ_{xx} and λ_{zz}, which can be separately fit to ρ_{xx} and ρ_{zz}. The Bloch-Grüneisen curves of Fig. (6) use Θ_D=750K, taken from low T specific heat of the neighboring compound TiO_2 [39]. Using the calculated plasma frequencies of Table I, we find $\lambda_{xx}\approx 0.8$ and $\lambda_{zz}\approx 0.9$. These values are a little higher than found in typical oxide metals (compare $\lambda\approx 0.45$ in RuO_2 [40].) The values of λ are reduced by a factor of 2 if we fit using Θ_D=500K, which characterizes the specific heat of TiO_2 in the range 15-65K [39], and is an equally reasonable choice. The corresponding Bloch-Grüneisen curves deviate from the measured $\rho(T)$ at $T>125$K instead of $T>190$K seen in Fig. (6). In either case, because of the small Fermi velocities, the corresponding ℓ values get small at higher T.

The mean free path has no unique definition. Previously we used $\ell=\langle\vec{v}^2\rangle^{1/2}\tau$, but an equally good choice is $\ell=\langle\vec{v}^2\rangle\tau/\langle|\vec{v}|\rangle$. In ferromagnetic CrO_2 we find $\langle\vec{v}^2\rangle^{1/2}=2.5\times10^5$m/s and $\langle|\vec{v}|\rangle=2.2\times10^5$m/s, so the two definitions differ by an unimportant amount. Boltzmann theory gives the following approximate relation:

$$\ell=\frac{\sum\vec{v}_k^2\tau\delta(\epsilon_k)}{\sum|\vec{v}_k|\delta(\epsilon_k)}\cong\frac{(2\pi)^3\hbar}{e^2}\frac{1}{A_{FS}^{\uparrow}+A_{FS}^{\downarrow}}\left(\frac{1}{\rho_{xx}}+\frac{1}{\rho_{yy}}+\frac{1}{\rho_{zz}}\right) \tag{4}$$

This provides a robust way to estimate mean-free paths, because the only theoretical input required is the area A_{FS}^s of the Fermi surface. Density functional theory has an excellent ability to give the correct shape of Fermi surface, even under conditions where the velocity of the quasiparticles at the Fermi surface, or the density of states, may be off. Our calculated areas are given in Table I. At low T, where ρ is only a few $\mu-\Omega$cm, ℓ in CrO_2 is hundreds of Angstroms. At T=200K, we estimate ℓ = 36Å. This is still the regime of a good band Fermi liquid. At higher T, the resistivity increases rapidly, and ℓ diminishes to $\approx$ 7Åat the Curie temperature, 390K. This number is estimated assuming the ferromagnetic electronic structure. If instead we use the paramagnetic Fermi surface, the area is much

larger and values of ℓ are reduced by a factor of 4.8 to sizes less than 2Å. This is the regime which has been called a "bad metal" by Kivelson and Emery [42]. In traditional bad metals like A15 structure intermetallics (Nb_3Sn, etc.) the resistivity is temperature-independent at this point, but in "exotic bad metals" like the high T_c superconductors, resistivity continues to rise even though propagating quasiparticle states of the Landau type cannot be present. Earlier [41] we found that the high T metallic (rutile structure) phase of VO_2 was also a "bad metal" in the "exotic" sense, and also the ferromagnet $SrRuO_3$ [24], so it should not be surprising if CrO_2 is also.

It is interesting to think about the nature of scattering in CrO_2 at temperatures near T_C. Figure (6) suggests that roughly half the scattering involves spin flips caused by spin fluctuations. The mean distance between spin-flip scatterings is $\approx \sqrt{2}\ell$, or 10Å. A spin flip takes an electron off the majority (up) spin Fermi surface into an insulating gap. It cannot remain there long unless joined by a sufficient number of other flipped electrons such that the local majority has changed spin direction and the down spins are now metallic with a Fermi surface leaving up spins insulating. Thus it is easy to imagine that the scattering is not completely incoherent, but has a collective feature. As temperature rises to near the Curie temperature, the bulk magnetization decreases primarily through fluctuating formation of opposite spin domains. It seems natural to associate the spin-flip scattering length with the size of these domains. Above T_C the same picture can be used, except that now the volume fraction of up and down domains is equal. Within each domain, electrons roughly behave as if they had the ferromagnetic band structure, with majority spin electrons having a Fermi surface, but badly lifetime-broadened. With a 10Åspin-flip mean-free path, and a 7Åtotal mean free path, the local Fermi liquid picture is close to total destruction. Looking at the resistivity shown in Fig. (6), it is hard to tell whether the resistivity is saturating or not. Additional measurements at higher T would be interesting.

ACKNOWLEDGMENTS

We thank R. J. Gambino and W. E. Pickett for useful advice. This work was supported in part by NSF grant no. DMR-9417755, and by the Division of Materials Sciences, U. S. Department of Energy, under contract DE-AC02-76CH00016. Computational support was provided by the Pittsburgh Supercomputer Center.

---

[1] K. Schwarz, J. Phys. F **16**, L211 (1986).
[2] R. A. De Groot, F. M. Mueller, P. G. van Engen, and K. H. J. Buschow, Phys. Rev. Letters **50**, 2024 (1983).
[3] K. P. Kämper, W. Schmitt, G. Güntherodt, R. J. Gambino, and R. Ruf, Phys. Rev. Letters **59**, 2788 (1987).
[4] R. Wiesendanger, H.-J. Güntherodt, G. Güntherodt, R. J. Gambino, and R. Ruf, Phys. Rev. Letters **65**, 247 (1990).
[5] H. Brändle, D. Weller, J. C. Scott, J. Sticht, P. M. Oppeneer, and G. Güntherodt, Int. J. Mod. Phys. **B7**, 345 (1993).
[6] E. Kulatov and I. I. Mazin, J. Phys. Condens. Matter **2**, 343 (1990).
[7] S. Matar, G. Demazeau, J. Sticht, V. Eyert, and J. Kübler, J. Phys. I France **2**, 315 (1992).
[8] A. V. Nikolaev and B. V. Andreev, Sov. Phys. – Solid State **35**, 603 (1993).
[9] O. Gunnarson and B. I. Lundqvist, Phys. Rev. B **13**, 4274 (1976).
[10] P. Hohenberg and W. Kohn, Phys. Rev. **136**, B864 (1964); W. Kohn and L. J. Sham, Phys. Rev. **140**, A1133 (1965).
[11] D. M. Ceperley and B. J. Alder, Phys. Rev. Lett. **45**, 566 (1980); J. Perdew and A. Zunger, Phys. Rev. B **23**, 5048 (1981).
[12] N. Troullier and J. L. Martins, Phys. Rev. B **43**, 1993 (1991).
[13] D. R. Hamann, M. Schlüter, C. Chiang, Phys. Rev. Lett. **43**, 1494 (1979).
[14] T. Sasaki, A. M. Rappe, and S. G. Louie, Sci. Rep. RITU **A39**, 37 (1993); Phys. Rev. B **52**, 12760 (1995).
[15] S. G. Louie, S. Froyen, and M. L. Cohen, Phys. Rev. B **26**, 1738 (1982).
[16] P. Porta, M. Marezio, J. P. Remeika, and P. D. Dernier, Mater. Res. Bull. **7**, 157 (1972).
[17] G. Lehmann and M. Taut, Phys. Stat. Sol. (b) **54**, 469 (1972).
[18] H. Brändle, D. Weller, S. S. P. Parkin, J. C. Scott, P. Fumagalli, W. Reim, R. J. Gambino, R. Ruf, and G. Güntherodt, Phys. Rev. B **46**, 13889 (1992).
[19] D. S. Redbell, J. M. Lommel, and R. C. DeVries, J. Phys. Soc. Japan **21**, 2430 (1966).
[20] N. Schubert and E. Wassermann, (unpublished); data quoted in ref. [18].
[21] P. I. Sorantin and K. Schwarz, Inorg. Chem. **31**, 567 (1992).
[22] J. K. Burdette, G. J. Miller, J. W. Richardson, Jr., and J. V. Smith, J. Am. Chem. Soc. **110**, 8064 (1988).
[23] V. Yu. Irkhin and M. I. Katsnel'son, Physics – Uspekhi **37**, 659 (1994).
[24] P. B. Allen, H. Berger, O. Chauvet, L. Forro, T. Jarlborg, A. Junod, B. Revaz, and G. Santi, Phys. Rev. B **53**, 4393 (1996).

[25] Y. Maeno, H. Hashimoto, K. Yoshida, S. Nishizaki, T. Fujita, J. G. Bednorz, and F. Lichtenberg, Nature (London) **372**, 532 (1994); T. Oguchi, Phys. Rev. B **51**, 1385 (1995); D. J. Singh, *ibid*, **52**, 1358 (1995).
[26] I. A. Campbell and A. Fert, in *Ferromagnetic Materials*, edited by E. P. Wohlfarth (North-Holland, Amsterdam, 1982), vol. 3, Ch. 9, pp747-804.
[27] B. L. Chamberland, Mat. Res. Bull. **2**, 827 (1967).
[28] G. K. White and S. B. Woods, Phil. Trans. Roy. Soc. **A 251**, 273 (1959).
[29] M. J. Laubitz, T. Matsumura, and P. J. Kelly, Can. J. Phys. **54**, 92 (1976).
[30] R. W. Powell, R. P. Tye, and M. J. Hichmann, Int. J. Heat Mass Transf. **8**, 679 (1965).
[31] W. F. Roeser and H. T. Wensel, *Temperature, its Measurement and Control in Science and Industry*, (Reinhold, New York, 1941) p.1312.
[32] J. M. Abraham, C. Tete, and B. Deviot, J. Less Common Metals **37**, 181 (1974).
[33] D. A. Papaconstantopoulos, *Handbook of the Band Structures of Elemental Solids* (Plenum, New York, 1986).
[34] C. Kittel, *Introduction to Solid State Physics*, 7th Ed. (Wiley, New York, 1996).
[35] E. L. Wolf, J. Zasadzinski, G. B. Arnold, D. F. Moore, J. M. Rowell, and M. R. Beasley, Phys. Rev. **B 22**, 1214 (1980).
[36] P. B. Allen, in *Superconductivity in d- and f-Band Metals*, H. Suhl and M.B. Maple, eds. (Academic Press, NY 1980) pp. 291-304.
[37] P. B. Allen, Phys. Rev. B **36**, 2920-23 (1987).
[38] J. Yamashita, S. Wakoh, and S. Asano, J. Phys. Soc. Jpn. **39**, 344 (1975).
[39] T. R. Sandin and P. H. Keesom, Phys. Rev. **177**, 1370 (1969).
[40] K. M. Glassford and J. R. Chelikowsky, Phys. Rev. **B 49**, 7107 (1994).
[41] W. Schulz, L. Forro, C. Kendziora, R. Wentzcovitch, D. Mandrus, L. Mihaly, and P.B. Allen, Phys. Rev. B, **46**, 14001-4 (1992).
[42] V. J. Emery and S. A. Kivelson, Phys. Rev. Lett. **74**, 3253 (1995).

TABLE I. Measured, calculated, and derived properties of CrO_2

Quantity	Ferromagnetic	Paramagnetic
	Experimental Values	
a (Å) (Ref. [16])	4.419	
c (Å)	2.912	
u	0.303	
γ (mJ/mole K) (Ref. [18])	7	
ρ(0K) ($\mu\Omega$cm)(Ref. [19])	≈ 5	
ρ(300K)	250	
ρ(500K)		570
	Theoretical Values	
u	0.3043	
$\omega(A_{1g})$ (cm^{-1})	587	
N(0) (states/eV/spin/CrO_2)	0.69	2.35
$\sqrt{\langle v_{Fx}^2 \rangle}$ (10^5m/s)	1.38	0.62
$\sqrt{\langle v_{Fz}^2 \rangle}$	1.56	0.79
Ω_{pxx} (eV)	1.91	2.22
Ω_{pzz}	2.15	2.84
Fermi Surface Area (Å^{-2})	8.86	21.43
	Derived Values	
$1 + \lambda_\gamma = N_\gamma(0)/N(0)$	4.3	
mean free path, ℓ(5K) (Å)	700	
ℓ(300K)	14	
ℓ(500K)		1.3